Electrochemical analysis of the reaction mechanism of sulfur reduction as a function of state of charge

Patrick Schön [a, b], Frederik Hintz [a], Ulrike Krewer [a, b, *]

[a] Technische Universitat Braunschweig, Institute of Energy and Process Systems Engineering, Franz-Liszt-Straße 35, 38106 Braunschweig, Germany
[b] Technische Universitat Braunschweig, Battery LabFactory Braunschweig, Langer Kamp 19, 38106 Braunschweig, Germany

ARTICLE INFO

Keywords:
Cyclic voltammetry
Discharge
Li-sulfur battery

ABSTRACT

Although being crucial for developing high capacity and long lasting lithium sulfur batteries, the discharge chemistry of the sulfur electrode is debated. In this study we examine a three electrode system with a glassy carbon working electrode immersed in electrolyte solution containing elemental sulfur as reactant and 1,3 dioxolane:1,2 dimethoxyethane with bis triflourmethansulfonimid lithium salt electrolyte.

We present essential new quantitative insights into the reaction steps occurring at the sulfur electrode of a lithium sulfur battery during discharge. The conducted sequence of electrochemical experiments allow to study the complex phenomena with classical electrochemical methods of cyclic voltametry, open circuit potential measurements and discharge. Our experimental analysis at different states of charge reveals the important role of chemical disproportionation to cell relaxation. The reduction re actions, their reversibility and the electrode performance strongly depend on the chemical equilibrium between the polysulfides. These results allow to formulate surround experimentally validated non formal reaction kinetic models. These give detailed information of the complex interaction of chemical and electrochemical reactions.

1. Introduction

Modern mobile devices and electric vehicles are increasingly dependent on electrical storage of energy to meet consumer de mands like in operation time or driving range. Current lithium ion battery technology is not able to satisfy the needs in energy density and power, cost and safety and toxicity, which drives the devel opment of a new generation of batteries [1–3]. With superior theoretical values in capacity (1672 mA h g^{-1}), gravimetric (2567 W h kg^{-1}) and volumetric energy density (2199 W h L^{-1}, based on the sum of the volumes of Li at the beginning and lithium sulfide (Li_2S) at the end of discharge) ithiumsulfur batteries (LSB) pose a promising new generation technology replacing lithium ion batteries (LIB) [4,5]. Exploiting this technology, practical energy densities of 500–600 W h kg^{-1} on a cell level become achievable, while being low in price and toxicity [6].

However, the potential of the sulfur electrodes is not well exploited yet because of low sulfur utilization on the higher po tential discharge plateau [7]. Furthermore, the breakthrough is still hindered by low cycleability because of rapid capacity fade due to degradation [8–10]. Contributing to this, the lithium (Li) anode gets corroded and polarized by insoluble Li_2S and lithium disulfide (Li_2S_2) due to the shuttle phenomenon that is initiated once soluble polysulfides are able to diffuse through the separator. This leads to self discharge and low coulombic efficiencies [11,12]. In addition, formation of insulating lithium sulfur (Li S) layers on the anode result in increasing internal resistances that prohibit high rate capability [13] and also active material loss [14–16]. A detailed knowledge of the sulfur reduction mechanism will help to improve the overall battery performance by identifying those limitations in reactions and transport processes. The general discharge/charge characteristics and the exact pathway of (S_8) reduction and sub sequent reactions are still uncertain and under investigation. Re searchers have not yet agreed on the multi step mechanism nor have they presented experimentally validated quantitative reaction kinetic models of S_8 reduction and polysulfide reactions.

The chemistry of the LSB is based on the lithium sulfur redox

* Corresponding author. Technische Universitat Braunschweig, Institute of Energy and Process Systems Engineering, Franz-Liszt-Straße 35, 38106 Braunschweig, Germany.
E-mail address: u.krewer@tu-braunschweig.de (U. Krewer).

reaction:

$$16\,Li + S_8 \rightleftharpoons 8\,Li_2S \tag{1}$$

The complete conversion of S_8 to Li_2S releases 16 e^- and characteristically exhibits two discharge plateaus. In a typical LSB, the cathode consists of a sulfur carbon composite material, a polymer or liquid electrolyte and a Li anode. Initially, S_8 dissolves into the electrolyte (Eq. (2)) and reacts at the electrochemically active surface sites (Eq. (3)):

$$S_{8(s)} \rightleftharpoons S_8 \tag{2}$$

$$S_8 + 2e^- \rightleftharpoons S_8^{2-} \tag{3}$$

The anodic reaction is

$$Li_{(s)} \rightleftharpoons Li^+ + e^- \tag{4}$$

This leads to the overall initial reaction at the cathode:

$$S_{8(s)} + 2e^- + 2Li^+ \rightleftharpoons Li_2S_8 \tag{5}$$

Afterwards various electrochemical and chemical disproportionation reactions are possible to reach the final reduction product of Li_2S. In general the electrochemical reactions can be expressed as:

$$S_n^{2-} + 2e^- \rightleftharpoons S_m^{2-} + S_{n-m}^{2-} \tag{6}$$

$$S_n^{2-} + 2(n/m \quad 1)e^- \rightleftharpoons (n/m)S_m^{2-} \tag{7}$$

where $n \in [2,8]$ and $m \mid m \in [1,7] \wedge (m < n) \wedge (m \geq 1)$. The chemical disproportionation reactions between polysulfides follow the general reaction scheme:

$$S_n^{2-} + S_m^{2-} \rightleftharpoons S_{n+x}^{2-} + S_{m-x}^{2-} \tag{8}$$

where $n \in [2,7]$, $m \mid (m \in [2,7]) \wedge (m \leq n)$ and $x \mid x \in [1,3] \wedge (x \leq n \quad 8) \wedge (x \leq 1 \quad m)$. Reactions of polysulfides with S_8 are also likely as shown by Berger et al. [17] and could follow the reaction scheme:

$$n/8\ S_8 + S_m^{2-} \rightleftharpoons S_{n+m}^{2-} \tag{9}$$

where $m \in [1,7]$ and $n \mid n \in [1,7] \wedge (n \leq 8 \quad m)$. Additionally, these reactions are competing with chemical redox reactions described in Eq. (10), that can occur between polysulfides and Li of the anode.

$$(n \quad 1)Li_2S_n + 2Li_{(s)} \rightarrow nLi_2S_{n-1} \tag{10}$$

where $n \in [2,8]$. Polysulfides with short chain lengths ($n \quad 2 \quad 5$) can be formed stably in solution. The Gibbs free energy of the polysulfide anions is so close that these anions are co existing in the solution [10]. Eqs. (2)–(10) yield a wide range of theoretically possible reactions mechanisms and intermediates which are subject of discussion.

The ongoing reactions including mechanisms and kinetics have been under investigation by various research groups using a large number of electrochemical methods like impedance spectroscopy [18,19], cyclic voltammetry (CV) [20,21] and rotating disk electrode setups [21]. In addition, a large number of chemical analysis methods were used to address the change of the LSB system during discharge and charge and to identify changes of the electrode surface or reacting species. These include ex situ investigations like high pressure liquid chromatography with a UV or mass spectrometer (HPLC/UV/MS) [22,23] and in situ measurements using UV–visible absorption spectroscopy (UV–vis) [24], X ray absorption near edge spectroscopy (XANES) [25,26], X ray diffraction (XRD) [12,27–29], X ray transmission microscopy (TXM) [28], nuclear magnetic resonance (NMR) and raman spectroscopy [12,30–33].

Wild et al. [6] summarized the published experimental and also modeling results and proposed a simplified model of the discharge mechanism that results in the characteristic two plateau discharge curve. The proposed mechanism will be discussed in the following as an example of the various reaction paths proposed.

The higher potential discharge plateau at around 2.3 V vs Li/Li_+ occurs because of two reduction steps that consume four electrons in total. After dissolution, the first electrochemical step that reduces S_8 is assumed to be equivalent to the initial reaction Eq. (5). The second reduction step takes place either as in Eq. (11) or Eq. (12):

$$Li_2S_8 + 2e^- + 2Li^+ \rightleftharpoons Li_2S_6 + Li_2S_2 \tag{11}$$

$$Li_2S_8 + 2e^- + 2Li^+ \rightleftharpoons 2Li_2S_4 \tag{12}$$

The main part of the electric charge is liberated on a lower level of around 2.0 V. On this lower potential discharge plateau electrochemical reaction Eq. (14) is assumed to proceed via a radical that is generated in the chemical reaction according to Eq. (13).

$$Li_2S_6 \leftrightharpoons 2LiS_3\cdot \tag{13}$$

$$LiS_3\cdot + e^- + Li \rightarrow Li_2S_3 \tag{14}$$

The product Li_2S_3 may react with the reactant of Eq. (13) by association and precipitation according:

$$Li_2S_3 + Li_2S_4 \rightleftharpoons Li_2S_6 + Li_2S_{(s)} \tag{15}$$

The proposed reaction mechanism by Wild et al. contains thus besides parallel and sequential steps also circular routes and thus would allow to explain the complex relaxation behavior observed when switching from operation to open circuit potential (OCP). There is to our knowledge no systematic experimental electrochemical study which gives an insight into the changes of the chemical and electrochemical reaction kinetics during discharge. To pave the way for more quantitative analysis and also simulation, we here present a sequence of electrochemical experiments that allows to study the complex phenomena with classical electrochemical methods. It is shown how the combination of CV, OCP and discharge reveals quantitative insights into the interplay of various chemical and electrochemical reactions and their progression over time. Based on our results we propose a mechanism including chemical and electrochemical steps as function of state of charge. Note that we will give detailed peak currents to facilitate quantitative modeling.

2. Experimental set-up

2.1. Preparation and cell setup

For the electrochemical investigations, a sealed three electrode set up with 12 ml volume was used. A glassy carbon disk electrode with 5 mm in diameter (Pine Research Instrumentation, Durham, NC) was used as working electrode. Counter and reference electrode consisted of Li metal (99.9%, Merck KGaA). 1,3 Dioxolan (DOL)

and 1,2 Dimethoxyethan (DME) and Bis triflourmethansulfonimid lithium salt (LiTFSI) salt, Merck KGaA, were used without any further treatment. The electrolyte was made by mixing DOL and DME in equal volumetric parts with 1 M LiTFSI inside an argon filled glovebox. Elemental S_8 (99.9%, Merck KGaA) was then dissolved into the electrolyte and stirred overnight to reach a 4 mM solution. Finally the cell was assembled and the electrodes were immersed into the electrolyte.

The electrochemical experiments were conducted in an argon atmosphere at room temperature of 25 °C using a Gamry Instruments Reference 3000 potentiostat. All working potentials are displayed vs. the Li reference electrode.

2.2. Electrochemical measurements

CVs were recorded in an unstirred and fresh solution with scan rates of 15 mV s^{-1}, 25 mV s^{-1}, 50 mV s^{-1}, 100 mV s^{-1} in a potential range of 3.8 V−1 V. After running five cycles, the scan rate was changed to the subsequent. Only the second cycle for each scan rate is used for analysis.

For discharge experiments, a constant current of 70 µA (5.69 mA g^{-1}) was applied. The cell was stirred with a magnetic stirrer to hinder early transport limitations.

The measurement sequence to characterize electrode state for different states of charges of the S_8 electrode is given in Fig. 1. Starting from the assembled cell, we recorded CVs with a scan rate of 50 mV s^{-1} for three cycles in a potential range of 3.8 V−1 V unstirred. Again, the second cycle is used for analyses. Following an equilibration time of 20 min at OCP the cell is discharged for one hour at 70 µA. In case that the potential of the cell remains above 0.6 V during discharge, a second longer equilibration at OCP is conducted with a duration of 40 min. After this, the measurement cycle restarts with a CV. The cycle is continued until potential during reaches 0.6 V, which is defined as the truncation condition. The whole experiment in this configuration allowed to record 19 subsequent cycles.

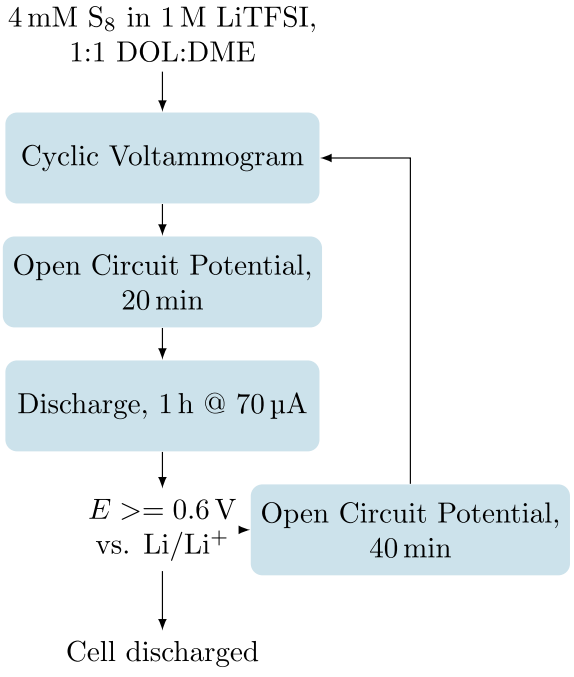

Fig. 1. Experimental procedure for electrochemical characterization of the discharge process at the glassy carbon electrode.

3. Results and discussion

3.1. Cyclic voltammetry

Before analyzing state of charge (SOC) influence, the electrode kinetics of the fresh solution is studied with CV as a reference point. As shown in Fig. 2a, the cathodic current at all scan rates increases at about 2.45 V. With increasing scan rates the peak potentials of the first cathodic peak decrease: 2.28 V; 2.25 V; 2.21 V and 2.21 V, whereas the cathodic peak current increase significantly: 157.35 µA, 238.18 µA, 337.21 µA and 428.94 µA.

For both peaks, the increase of the scan rate causes not only the expected increase in peak current but also a slight shift of the peaks to lower potentials.

In contrast to the reduction, only one peak is observed in the oxidation part of the CV. The given peak potentials are 2.63 V, 2.66 V, 2.68 V and 2.69 V with peak currents of 62.17 µA,162.41 µA, 282.55 µA and 401.03 µA. Similar to the reduction, the peak currents are increasing with increasing scan rate. The anodic peak potentials shift to higher values. At 50 mV s^{-1} the stagnant glassy carbon electrode shows the same behavior for a 1:1 DOL:DME with 1 M LiTFSI electrolyte and 4 mM S_8 as previously reported by Ref. [21]. They have attributed the first and second cathodic peak to the reactions given in Eq. (3), i.e. production of S_8^{2-} and Eq. (12) production of S S_4^{2-}. The S S_8^{4-} anion is not considered as it is believed to have only a short lifetime in low dielectric solvents, reacting directly to S S_4^{2-} with similar magnitude as the reaction to S S_8^{2-}.

The authors variation in scan rate allows to get additional information to possible chemical reactions. Indeed, the relation between anodic and cathodic peak currents $i_{p,a}/i_{p,c}$ increases with

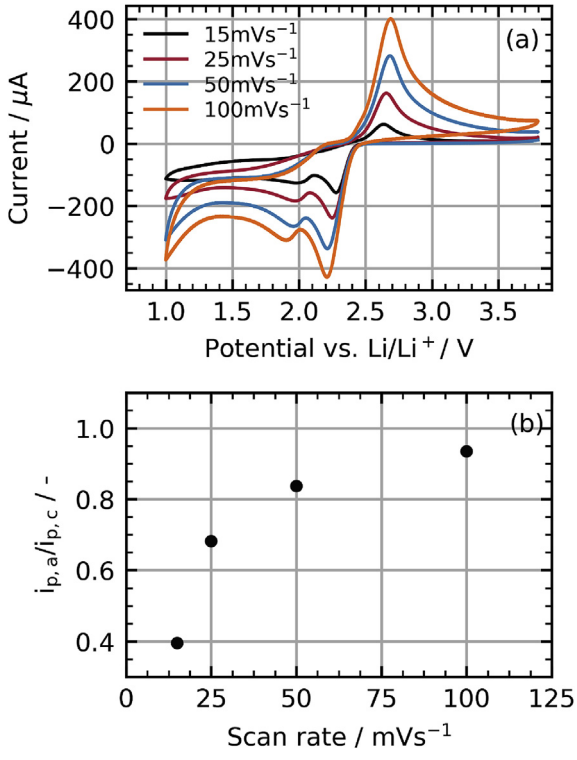

Fig. 2. (a)CVs of the glassy carbon electrode in 1:1 DOL: DME, 1 M LiTFSI electrolyte at scan rates of 15 mV s^{-1} to 100 mV s^{-1}. (b) Ratio of anodic peak current $i_{p,a}$ to cathodic peak current $i_{p,c}$ of the first peak at different scan rates.

scan rate as indicated in Fig. 2b. The low ratio of anodic to cathodic current for low scan rates suggests that a chemical reactions, e.g. as in Eq. (8) oxidize the electrochemically oxidizeable species with a certain rate [34]. Furthermore, the current reaches ~0 μA at the backward sweep after the potential 2.2 V where reactions causing the second cathodic peak are no longer causing a current. The electrochemical reaction of diffusing substrate to the surface is hindered, therefore a chemical reaction between S_8 and poly sulfides following the scheme in Eq. (9) must be present.

The above given experiment resembles a full state of charge, without accumulation of large amounts of intermediates. Reactions of such species may be observable mostly at lower state of charge. Thus, in later sections the authors analyze the CVs for various states of charge during the discharge process to evaluate possible changes in species and reactions.

3.2. Cell discharge

Before conducting CVs at various state of charge, the discharge behavior without disturbance by CV and OCP should be recorded as a reference. We carried out the discharge experiment in the stirred cell. The discharge curve, shown in Fig. 3, reveals two plateaus. The higher potential discharge plateau is at a potential of 2.36 V–2.28 V and ends at a capacity of ca. 100 mA h g^{-1}. The lower plateau has a potential between 2.13 V and 2.00 V and yields an additional capacity of ca. 80 mA h g^{-1}. In between these plateaus is a transition phase starting at 2.28 V until 2.13 V with a capacity of ca. 30 mA h g^{-1}. In total the capacities add up to 238 mA h g^{-1}. This corresponds to 14.23% of the theoretical value of 1672 mA h g^{-1} for the complete reduction of the dissolved S_8. There are various reasons for the low capacity of the cell that are well known in the literature [35], e.g. the formation of Li_2S_2 and Li_2S which block the electrode surface and transport limitations. The low ratio of active area to volume of reactants for our setup may explain the very low values observed here.

The two plateaus in Fig. 3 can be attributed to different electrochemical reactions that take place at different standard potentials. The first plateau corresponds to the first peak observed in the CV because of similar potentials. To further analyze the reactions, the discharge is combined with CV measurements in the procedure displayed in Fig. 1.

3.3. Open circuit and cyclic voltametry at different states of charge

The results of this combined experiment of OCP, CV and discharge measurements are shown in Figs. 4 and 5. Fig. 4 a and b

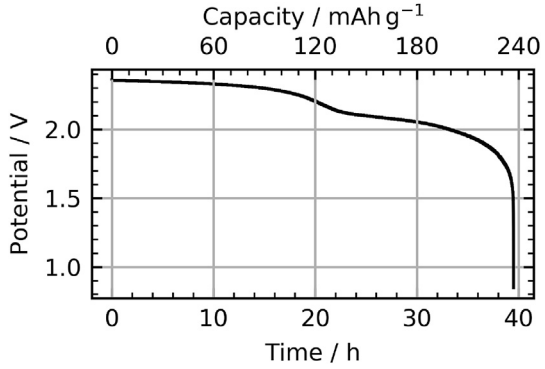

Fig. 3. Discharge experiment with a cathodic current of 70 μA in the stirred three electrode cell. Reduction was performed at a glassy carbon electrode in 4 mM S_8 1.0 M LiTFSI, 1:1 DOL:DME.

display the current and potential behavior of the cell during cycle ten, which is used for illustration of the method. Directly after completing the discharge part of cycle nine, the progression of OCP vs. time of cycle ten can be studied. It is increasing from 2.365 V for ca. 10 min until it reaches a constant potential of 2.42 V. The subsequent CV is recorded from this equilibrium state. After the CV measurement, the OCP does not show any noticeable shift in potential, suggesting that no major changes occurred in solution or electrode due to CV or further equilibration during CV. The last step of the exemplary cycle is the discharge of the cell, where the potential drops fast at the beginning and reaches a lower gradient of 3.17 μA h^{-1} afterwards.

Fig. 4c displays the OCP in the period prior to the CVs for all cycles. The behavior of each individual cycle, except for the first, is similar to the tenth, showing a rapid relaxation to higher potential and subsequent equilibration. The equilibrium value of the OCP is decreasing monotonously in the course of cycles. In contrast, the initial OCP values observed directly after the discharge sequence differ strongly and pass through a local minimum at the tenth cycle. These differences in relaxation behavior strongly indicate changes in the prevalent species and in the chemical reactions taking place during discharge. Overall, the monotonously decreasing equilibrium OCP indicates that the present polysulfides in solution causing the mixed potential are continuously decreasing in length. The initial OCP is strongly affected by the presence of medium size polysulfides directly after discharge. These disproportionate to longer and shorter polysulfides according to Eq. (8) or are reacting with S_8 to longer polysulfides according to Eq. (9) leading to the observed relaxation behavior. The amount of relaxation in the OCP has a local maximum around the tenth cycle revealing the strongest influence of disproportionation in this cycle. Thus, the overall concentration of polysulfide during discharge reaches a maximum where also the initial OCP has a local minimum. Subsequently, the amount of short polysulfides in solution decreases resulting in the increasing initial OCP because longer chain polysulfides gain more influence on the mixed potential. The decreasing concentration of short polysulfides can be explained by the production of S^{2-} by disproportionation and its precipitation, as suggested by Ref. [36] This is also supported by the fact that relaxation behavior decreases, implying that the solution is closer to equilibrium after discharge. The chemical equilibrium has shifted to shorter polysulfides explaining lower equilibrium OCP.

Based on these observations, the OCP reveals two phases of the sulfur reduction mechanism. In the first phase, the sulfur relaxation behavior increases and disproportionation of shorter polysulfides lead to long chain polysulfides. At the same time overall polysulfide concentration is increasing until reaching the local minimum in the initial OCP and the maximum in relaxation behavior. The second phase starts with the precipitating S^{2-} and the consequent decrease in polysulfide concentration in solution. Relaxation behavior decreases because the solution is closer to equilibrium after discharge.

The discharge potential shown in Fig. 4d can be divided in similar phases. The first seven cycles reveal no significant potential decrease during discharge. Maintaining this high discharge potential requires a sufficiently high concentration of long polysulfides. The initially dissolved amount of sulfur is the main factor here. Additionally, the OCP relaxation behavior revealed the important role of chemical production of long chain polysulfides during this discharge period to keep the OCP at high level. After this, the potential drops substantially at the beginning of discharge, reaching a lower value and is leveling off. In this second phase, the amount of long polysulfides is only sufficient to keep the potential high for a short instance. The main part of electrochemical reduction is caused by shorter polysulfides taking place at a lower

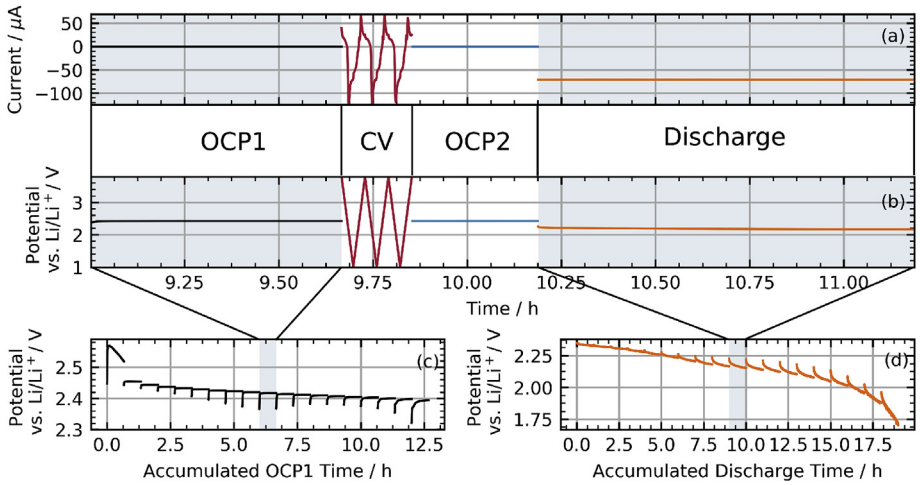

Fig. 4. Results of cycle ten of the combined OCP, CV and discharge experiment according to Fig. 1. (a) Measured current during the experiment, (b) measured potential during the experiment, (c) OCPs before the CV in all cycles, (d) discharge curves of all cycles of 1 h discharge.

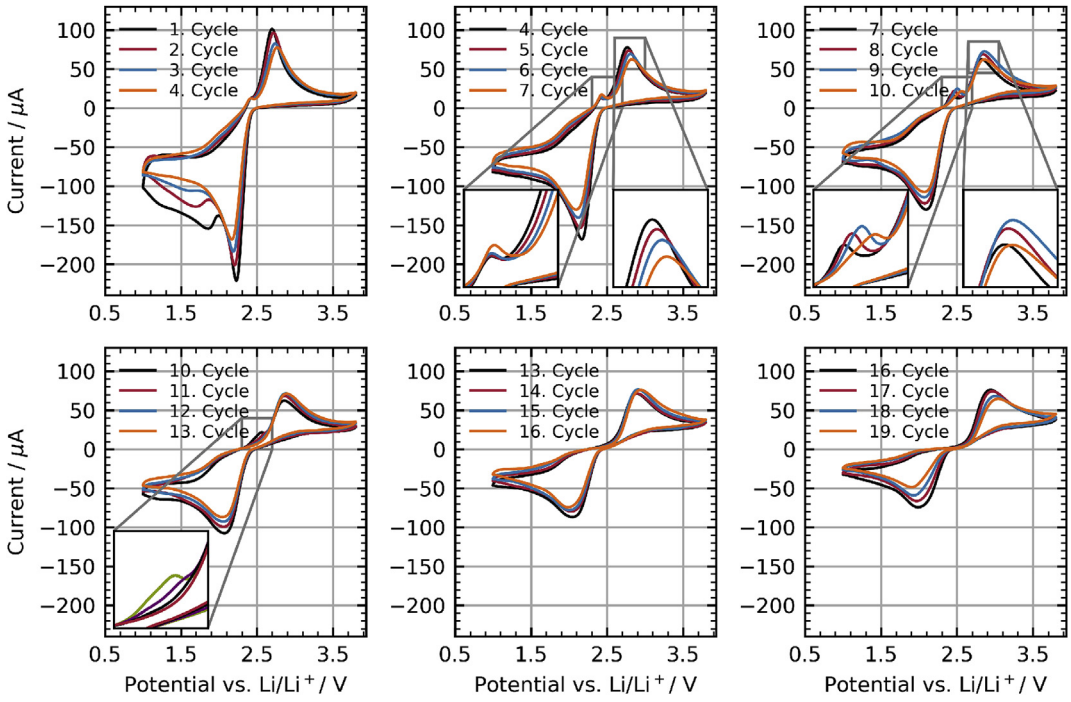

Fig. 5. CVs measured with a scan rate of 50 mV s ^{1} at different states of charge in a 1:1 DOL:DME with 1 M LiTFSI electrolyte and 4 mM S_8.

potential. Diffusion of S_8 to the surface might still be present, but due to chemical reactions with short polysulfides (Eq. (9)) poly sulfides are produced that react at a lower potential. Relaxation and diffusion during the OCP phases of each cycle create the long pol ysulfides that cause the initial high potential during discharge.

The observed phases revealed by the OCP and the discharge potential correspond to the higher and lower potential discharge plateaus of typical LSB that are also visible in Fig. 3. Therefore, cycle one to nine belong to the higher potential discharge plateau, cycle ten to 19 belong to the lower potential discharge plateau. We were already able to point out the important role of relaxation behavior in the mechanism. Analysis of the CVs will give a deeper insight into the occurring electrochemical reactions on the two plateaus.

CV is the second part of each cycle starting from the equilibrium potential with a scan rate of 50 mV s^{-1}. The results are displayed in Fig. 5. The qualitative shape of the initial CV of cycle one is similar to that of the CV experiment in Fig. 2a, initially showing two peaks during reduction and one during oxidation. Throughout the cycles of the higher potential discharge plateau, there is a steep increase of current at a potential of ca. 2.4 V which flattens only after the tenth cycle. The origin corresponds to the higher potential discharge plateau OCP. Thus, the following peak is caused by the main elec trochemical reaction of the higher potential discharge plateau. The peak current of the first cathodic peak decreases constantly for each cycle, while shifting to lower potentials. The general shape of the peak does not change, as it stays narrow. In contrast to the first peak, the second disappears after the third cycle. Both effects suggest a decrease of reactant concentration or in case of the

second peak, disappearance of certain species or inability of them to react electrochemically after the third cycle. This supports the finding and conclusion drawn from Fig. 2c and d, that on the higher potential discharge plateau the reaction mechanism is dominated by long polysulfide reduction.

In Fig. 5 the anodic current initially exhibits one anodic peak and a small plateau. After three cycles, the peak splits up into two separated peaks from cycle three to ten. The first peak appears at a peak potential of 2.43 V and has a peak current of 17.23 μA while the second appears at a peak potential of 2.74 V and has a peak current of 82.60 μA. Thus, two electrochemical reactions were initially overlapping and invisible in the conventional CV in Fig. 2. These are caused by electrochemical oxidation of short polysulfides. Their independence is obvious, due to the fact that the first peak disap pears in cycle eleven. We assume an association of the second cathodic peak and the first anodic peak, as the disappearance of the cathodic peak correlates with the separation into two anodic peaks, where the first decreased significantly. This also points to an elec trochemical reaction, that is unable to proceed.

During the lower potential discharge plateau, after cycle ten, the cathodic peak is getting broader, indicating overlapping electro chemical reactions. The origin has not changed because of the presence of long chain polysulfides that were formed through relaxation during OCP measurement. However, the former steep increase now flattens out and the peak potential is significantly shifted to lower potentials. Thus, the dominant electrochemical reactions are now due to shorter polysulfides as in Eq. (13). Due to low sulfur utilization on the higher potential discharge plateau S_8 is still diffusing to the electrochemical active electrode. High reac tivity of S_8 with polysulfides of short chain length reduces the amount to a point where there is no peak visible in the CVs.

The discharge experiment with CV was repeated with a varia tion of scan speeds in order to see if additional reactions may be visible that are covered at other scan rates. The resulting CVs are shown in Fig. 6. For all different scan rates, the reduction starts at the same potential of ca. 2.45 V. With increasing scan rate the po tential of the first peak shifts slightly to lower potentials and the current is strongly increasing. The second cathodic peak is only visible for a scan rate of 10 mV s^{-1} and 100 mV s^{-1}, at 1000 mV s^{-1} it disappears. The electrochemical reaction causing the cathodic current is dominant and overlaps the second at fast scan rates. Therefore, the process is either hindered by chemical reaction, a transport or an adsorption process that is not able to keep up with the scan rate. No further additional peaks are visible compared to 50 mV s^{-1}. The observed increase in peak current ratios for increasing scan rates in Fig. 2 gets confirmed by the results in Fig. 6a however this effect is distinct after 3 h and 8 h. Thus, the influence of chemical reactions decreases on the lower potential discharge plateau.

3.4. Reduction mechanism of sulfur

The differences between discharge curves with and without relaxation time and the relaxation behavior of the OCP as well as the CVs as a function of state of charge yield important information concerning the electrochemical reaction step, their interplay with chemical reactions and the prevalence of certain reactant species. Based on these observations, we propose a reaction mechanism discussed in the following. The first reaction appearing at the higher potential discharge plateau is attributed to dissolved S_8 reacting to S S_8^{2-} as already reported by Ref. [21].

$$S_8 + 2e^- \rightleftharpoons S_8^{2-} \tag{16}$$

A further step taking place at this plateau is the reduction of SR_8^{2-} to S_8^{4-} [21]. already assigned a short lifetime to S_8^{4-} in DOL:DME with LiTFSI electrolyte. Therefore, the S_8^{4-} molecule decomposes further into two S S_4^{2-}.

$$S_8^{2-} + 2e^- \rightleftharpoons S_8^{4-} \tag{17}$$

$$S_8^{4-} \rightarrow 2S_4^{2-} \tag{18}$$

Taking into account the potential relaxation behavior and decreasing ratio of the peak currents in Fig. 2b at decreasing scan rates, the chemical reactions have to have a strong influence and are diminishing the amount of S_4^{2-}. Referring to Eqs. (8) and (9) a chemical equilibrium will be reached by disproportionation of the S_4^{2-} ion and subsequent reactions [10]. identified S_2^{2-}, S_3^{2-} and S_4^{2-} to be the major intermediates because their existence is advanta geous, and [37] also named S_n^{2-} (n 2 5, 7, 8) to be the most stable. Thus, the system seeks towards an equilibrium of poly sulfides with longer and shorter chain length than initially present. The process of reaching this equilibrium seems to be relatively slow and is the cause of significant delay in establishing a stable OCP. The observed relaxation to almost the initial OCP is a good indicator for the production of long chain polysulfides, e.g. S_8^{2-}, and S_8 as they can be found at the start of discharge. At the minimum of the initial OCP, precipitation of S_{2-} is initiated which indicates the end of the higher potential discharge plateau.

After cycle ten, the recreated long polysulfides are present only at low concentrations and electrochemical reactions of shorter polysulfides become dominant as shown by the fast potential drop during discharge. The lower potential discharge plateau is therefore attributed to electrochemical reactions of short polysulfides as in Eq. (14); our studies here do not allow to identify a dominant re action. Diffusing S_8 is not reacting directly at the electrode, but reacting chemically with produced polysulfides as no peak caused

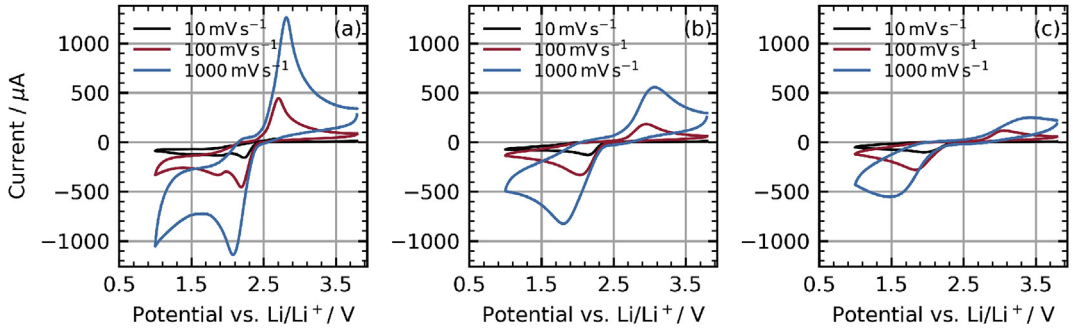

Fig. 6. CVs with scan rates of 10 mV s ^{1}, 100 mV s ^{1} and 1000 mV s ^{1} in the combined experiment with OCP measurements and discharge for a glassy carbon electrode at (a) initial state, (b) 3 h discharge and (c) 8 h discharge in a 1:1 DOL:DME with 1 M LiTFSI electrolyte and 4 mM S_8.

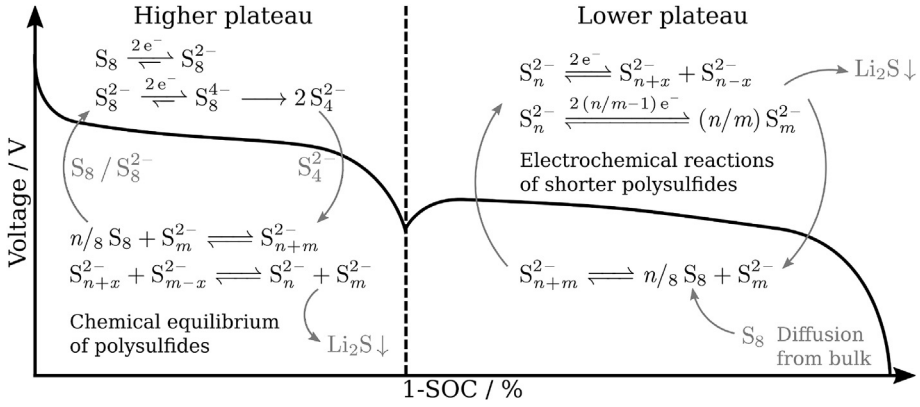

Fig. 7. Illustration of mechanism of electrochemical and chemical reactions as a function of state of charge.

by Eq. (3) is visible in CV at low SOC. The anodic and cathodic peak currents are almost equal in the CVs of the lower potential discharge plateau. Thus, these electrochemical reactions are reversible.

The OCP shows less relaxation behavior indicating, that the reduction products of the discharge phase are closer to chemical equilibrium. Fig. 7 shows the mechanism assumed to take place during discharge.

4. Conclusions

In this work we determined further details of the sulfur reduc tion mechanism by studying changes of relaxation behavior of CV and OCP during discharge. Analysis of CV at different states of charge with different scan rates gave valuable insights into the nature of reactants and reactions as a function of SOC.

The prevailing reduction reactions, their reversibility and the electrode performance strongly depend on the chemical dispro portionation and the equilibrium between the polysulfides. This is observable in the CV measurements and in the SOC specific relaxation behavior during the OCP measurements. Furthermore, the CV measurements during discharge showed the dependency of the electrochemical reactions on the SOC. While sulfur and long chain polysulfides are reacting on the higher potential discharge plateau, polysulfides with shorter chain length reduce at the po tential of the lower potential discharge plateau.

Additionally, the reaction is becoming more reversible in course of discharge showing the decreasing portion of worse oxidizeable species.

The presented insights and data now allow to formulate sound experimentally validated non formal reaction kinetic models. These would give a detailed quantitative insight into the complex interaction of chemical and electrochemical reactions. This again will allow in future to understand the state of LSB by applying simple dynamic electrochemical measurements.

Acknowledgements

The authors gratefully acknowledge the financial support of Volkswagen AG, Wolfsburg and Prof. Dr. Uwe Schroder of the Institute of Environmental and Sustainable Chemistry, Technische Universitat Braunschweig for his consultation.

References

[1] J.B. Goodenough, K.-S. Park, The Li-ion rechargeable battery: a perspective, J. Am. Chem. Soc. 135 (4) (2013) 1167 1176.
[2] J.B. Goodenough, A. Manthiram, A perspective on electrical energy storage, Mrs Commun. 4 (4) (2014) 135 142.
[3] B. Scrosati, J. Garche, Lithium batteries: status, prospects and future, J. Power Sources 195 (9) (2010) 2419 2430.
[4] X. Ji, L.F. Nazar, Advances in Li S batteries, J. Mater. Chem. 20 (44) (2010) 9821 9826.
[5] P.G. Bruce, S.A. Freunberger, L.J. Hardwick, J.-M. Tarascon, Li-O2 and Li-S batteries with high energy storage, Nat. Mater. 11 (1) (2012) 19.
[6] M. Wild, L. O'Neill, T. Zhang, R. Purkayastha, G. Minton, M. Marinescu, G. Offer, Lithium sulfur batteries, a mechanistic review, Energy Environ. Sci. 8 (12) (2015) 3477 3494.
[7] P. Titscher, P. Schon, M. Horst, U. Krewer, A. Kwade, Increasing energy densities of sulfur cathodes via dispersing and calendering processes for lithium-sulfur batteries, Energy Techno. 6 (6) (2018) 1139 1147.
[8] W. Xu, J. Wang, F. Ding, X. Chen, E. Nasybulin, Y. Zhang, J.-G. Zhang, Lithium metal anodes for rechargeable batteries, Energy Environ. Sci. 7 (2) (2014) 513 537.
[9] C. Zu, A. Manthiram, Stabilized lithium metal surface in a polysulfide-rich environment of lithium sulfur batteries, J. Phys. Chem. Lett. 5 (15) (2014) 2522 2527.
[10] R.S. Assary, L.A. Curtiss, J.S. Moore, Toward a molecular understanding of energetics in Li S batteries using nonaqueous electrolytes: a high-level quantum chemical study, J. Phys. Chem. C 118 (22) (2014) 11545 11558.
[11] Y. Diao, K. Xie, S. Xiong, X. Hong, Shuttle phenomenon the irreversible oxidation mechanism of sulfur active material in Li S battery, J. Power Sources 235 (2013) 181 186.
[12] J.-T. Yeon, J.-Y. Jang, J.-G. Han, J. Cho, K.T. Lee, N.-S. Choi, Raman spectroscopic and X-ray diffraction studies of sulfur composite electrodes during discharge and charge, J. Electrochem. Soc. 159 (8) (2012) A1308 A1314.
[13] D. Aurbach, E. Pollak, R. Elazari, G. Salitra, C.S. Kelley, J. Affinito, On the surface chemical aspects of very high energy density, rechargeable Li sulfur batteries, J. Electrochem. Soc. 156 (8) (2009) A694 A702.
[14] M. Lécuyer, J. Gaubicher, M. Deschamps, B. Lestriez, T. Brousse, D. Guyomard, Structural changes of a Li/S rechargeable cell in lithium metal polymer technology, J. Power Sources 241 (2013) 249 254.
[15] C.-S. Kim, A. Guerfi, P. Hovington, J. Trottier, C. Gagnon, F. Barray, A. Vijh, M. Armand, K. Zaghib, Importance of open pore structures with mechanical integrity in designing the cathode electrode for lithium sulfur batteries, J. Power Sources 241 (2013) 554 559.
[16] S.-H. Kang, X. Zhao, J. Manuel, H.-J. Ahn, K.-W. Kim, K.-K. Cho, J.-H. Ahn, Effect of sulfur loading on energy density of lithium sulfur batteries, Phys. Status Solidi (a) 211 (8) (2014) 1895 1899.
[17] A. Berger, A.T. Freiberg, A. Siebel, R. Thomas, M.U. Patel, M. Tromp, H.A. Gasteiger, Y. Gorlin, The importance of chemical reactions in the charging process of lithium-sulfur batteries, J. Electrochem. Soc. 165 (7) (2018) A1288 A1296.
[18] N.A. Canas, K. Hirose, B. Pascucci, N. Wagner, K.A. Friedrich, R. Hiesgen, Investigations of lithium sulfur batteries using electrochemical impedance spectroscopy, Electrochim. Acta 97 (2013) 42 51.
[19] Z. Deng, Z. Zhang, Y. Lai, J. Liu, J. Li, Y. Liu, Electrochemical impedance spectroscopy study of a lithium/sulfur battery: modeling and analysis of capacity fading, J. Electrochem. Soc. 160 (4) (2013) A553 A558.
[20] Y. Jung, S. Kim, B.-S. Kim, D.-H. Han, S.-M. Park, J. Kwak, Effect of organic solvents and electrode materials on electrochemical reduction of sulfur, Int. J. Electrochem. Sci. 3 (5) (2008) 566 577.
[21] Y.-C. Lu, Q. He, H.A. Gasteiger, Probing the lithium sulfur redox reactions: a rotating-ring disk electrode study, J. Phys. Chem. C 118 (11) (2014) 5733 5741.
[22] C. Barchasz, F. Molton, C. Duboc, J.-C. Leprêtre, S. Patoux, F. Alloin, Lithium/sulfur cell discharge mechanism: an original approach for intermediate species identification, Anal. Chem. 84 (9) (2012) 3973 3980.

[23] A. Kawase, S. Shirai, Y. Yamoto, R. Arakawa, T. Takata, Electrochemical reactions of lithium sulfur batteries: an analytical study using the organic conversion technique, Phys. Chem. Chem. Phys. 16 (20) (2014) 9344 9350.
[24] N.A. Canas, D.N. Fronczek, N. Wagner, A. Latz, K.A. Friedrich, Experimental and theoretical analysis of products and reaction intermediates of lithium sulfur batteries, J. Phys. Chem. C 118 (23) (2014) 12106 12114.
[25] J. Gao, M.A. Lowe, Y. Kiya, H.D. Abruna, Effects of liquid electrolytes on the charge discharge performance of rechargeable lithium/sulfur batteries: electrochemical and in-situ X-ray absorption spectroscopic studies, J. Phys. Chem. C 115 (50) (2011) 25132 25137.
[26] M. Cuisinier, P.-E. Cabelguen, S. Evers, G. He, M. Kolbeck, A. Garsuch, T. Bolin, M. Balasubramanian, L.F. Nazar, Sulfur speciation in Li S batteries determined by operando X-ray absorption spectroscopy, J. Phys. Chem. Lett. 4 (19) (2013) 3227 3232.
[27] M.A. Lowe, J. Gao, H.D. Abruna, Mechanistic insights into operational lithium sulfur batteries by in situ X-ray diffraction and absorption spectroscopy, RSC Adv. 4 (35) (2014) 18347 18353.
[28] J. Nelson, S. Misra, Y. Yang, A. Jackson, Y. Liu, H. Wang, H. Dai, J.C. Andrews, Y. Cui, M.F. Toney, In operando X-ray diffraction and transmission X-ray microscopy of lithium sulfur batteries, J. Am. Chem. Soc. 134 (14) (2012) 6337 6343.
[29] S. Waluś, C. Barchasz, J.-F. Colin, J.-F. Martin, E. Elkaïm, J.-C. Leprêtre, F. Alloin, New insight into the working mechanism of lithium sulfur batteries: in situ and operando X-ray diffraction characterization, Chem. Commun. 49 (72) (2013) 7899 7901.
[30] H.-L. Wu, L.A. Huff, J.L. Esbenshade, A.A. Gewirth, In situ EQCM study examining irreversible changes the sulfur carbon cathode in lithium sulfur batteries, ACS Appl. Mater. Interfaces 7 (37) (2015) 20820 20828.
[31] L.A. Huff, J.L. Rapp, J.A. Baughman, P.L. Rinaldi, A.A. Gewirth, Identification of lithium sulfur battery discharge products through 6 Li and 33 S solid-state MAS and 7 Li solution NMR spectroscopy, Surf. Sci. 631 (2015) 295 300.
[32] K.A. See, M. Leskes, J.M. Griffin, S. Britto, P.D. Matthews, A. Emly, A. Van der Ven, D.S. Wright, A.J. Morris, C.P. Grey, et al., Ab initio structure search and in situ 7Li NMR studies of discharge products in the Li S battery system, J. Am. Chem. Soc. 136 (46) (2014) 16368 16377.
[33] J. Xiao, J.Z. Hu, H. Chen, M. Vijayakumar, J. Zheng, H. Pan, E.D. Walter, M. Hu, X. Deng, J. Feng, et al., Following the transient reactions in lithium sulfur batteries using an in situ nuclear magnetic resonance technique, Nano Lett. 15 (5) (2015) 3309 3316.
[34] C.H. Hamann, W. Vielstich, Elektrochemie, Wiley-VCH-Verlag, 1998.
[35] V. Kolosnitsyn, E. Kuzmina, E. Karaseva, On the reasons for low sulphur utilization in the lithium sulphur batteries, J. Power Sources 274 (2015) 203 210.
[36] V. Kolosnitsyn, E. Kuzmina, E. Karaseva, S. Mochalov, A study of the electrochemical processes in lithium sulphur cells by impedance spectroscopy, J. Power Sources 196 (3) (2011) 1478 1482.
[37] L. Wang, T. Zhang, S. Yang, F. Cheng, J. Liang, J. Chen, A quantum-chemical study on the discharge reaction mechanism of lithium-sulfur batteries, J. Energy Chem. 22 (1) (2013) 72 77.